Maximum Allowable Current Determination of RBS By Using a Directed Graph Model and Greedy Algorithm

Binghui Xu[1†], Guangbin Hua[1†], Cheng Qian[1*], Quan Xia[1,2], Bo Sun[1], Yi Ren[1], and Zili Wang[1]

[1]School of Reliability and Systems Engineering, Beihang University, Beijing, 100191, China

[2]School of Aeronautic Science and Engineering at Beihang University, Beijing, China

[*]Address correspondence to: cqian@buaa.edu.cn

[†]These authors contributed equally to this work.

Abstract

Reconfigurable Battery Systems (RBSs) present a promising alternative to traditional battery systems due to their flexible and dynamically changeable topological structure subjected to battery charging and discharging strategies. During the operation of the RBS, the Maximum Allowable Current (MAC) of system that ensures each battery's current remains within a safe range, is a critical indicator to guide the system's reconfiguring control, ensuring its safety and reliability. In this paper, we firstly propose a calculation method for the MAC of arbitrary RBS using a greedy algorithm in conjunction with a directed graph model of the RBS. By introducing the shortest path of the battery, the greedy algorithm transforms the enumeration of switch states in the brute force algorithm into the combination of the shortest paths, which greatly increases the efficiency of the determination of the MAC. The directed graph model, based on the equivalent circuit, provides a specific method for calculating the MAC of a given structure. This method has been validated on two published 4-battery-RBSs and one with more complex structure. It obtaining the same results as the brute force algorithm method, while achieves significantly improved computational efficiency ($N_s 2^{N_s - N_b} \log N_b$ times faster than the brute force algorithm for a RBS with N_b batteries and N_s switches, theoretically). The main advantage of this method is its ability to calculate the MAC of RBSs with arbitrary structures, even in the scenarios with random isolated batteries.

1 Introduction

Battery Energy Storage Systems (BESSs) are extensively employed in various applications, such as wind power plants and space power systems, to store and release high-quality electrical energy [1–5]. Typically, a BESS consists of numerous batteries interconnected by series-parallel circuitry

1

to provide the required capacity storage. However, traditional BESSs, in which the batteries are connected in a fixed topology, exhibit a significant weakness in their worst battery due to the so-called cask effect. Moreover, if this worst battery fails from operation, it can exacerbate the degradation of other batteries with a high possibility, leading to reliability and safety issues [6–8]. These problems have become significant technical barriers in the development of new-generation space vehicles unfortunately [9].

Reconfigurable Battery System (RBS), which can dynamically switch to different circuit topology configurations as required, is expected to solve the above problems[10]. The ability of switching circuit helps to isolate unhealthy batteries, thereby improving the safety and reliability of the battery system. In order to illustrate the working principle of RBS, a typical RBS structure developed by Visairo [11](Figure 1a) is taken as an example to show the reconfiguration process. In this structure, the batteries can be connected not only in series when the switches S_1, S_5, S_6, S_7, S_8, S_9, and S_{13} are closed (Figure 1b), but also in parallel when S_1, S_2, S_3, S_4, S_5, S_9, S_{10}, S_{11}, S_{12}, and S_{13} are closed (Figure 1c). Furthermore, when an unhealthy battery, for instance the orange one B_3 in Figure 1d, appears in the RBS, it can be isolated by opening its two adjacent switches (i.e. S_4 and S_{11}), ensuring the system still remains a reliable working mode.
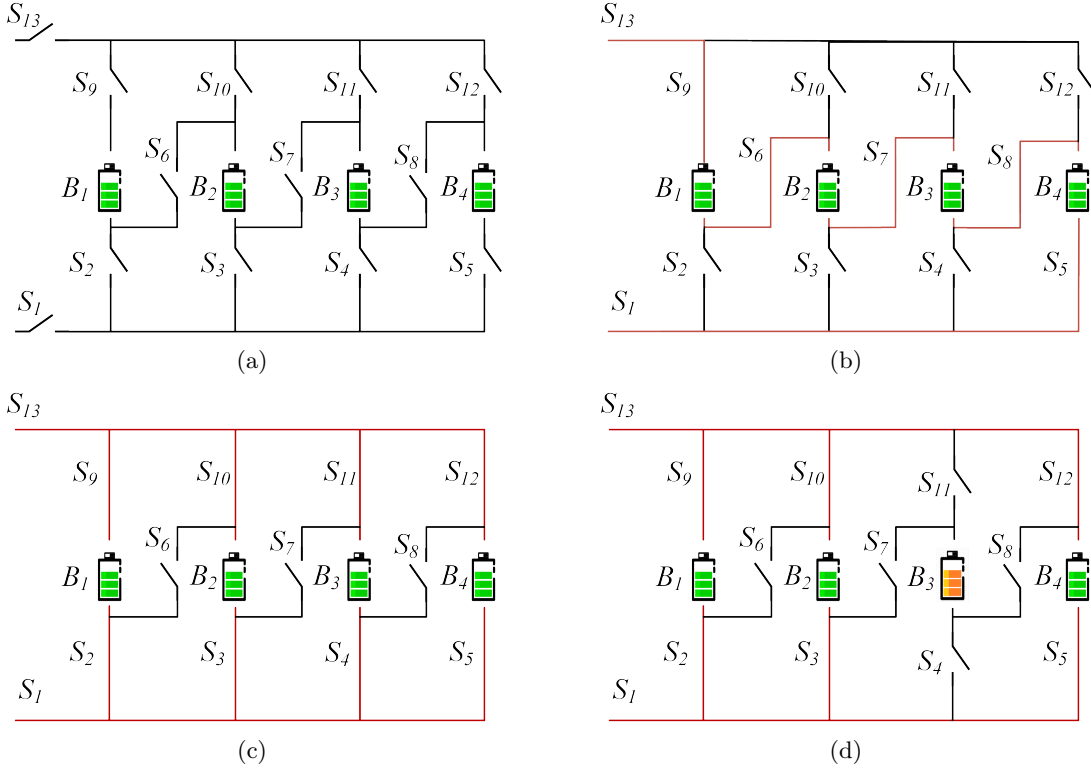

Figure 1: (a) The RBS structure proposed by Visairo[11], with all batteries in (b) series connection, (c) parallel connection, and (d) battery B_3 isolated.

Recently, various types of RBS with different flexibility and reconfigurability have been designed to meet application requirements. For example, Ci et al. [12] proposed a RBS structure that

can dynamically adjust the batteries discharge rate to fully exploit the available capacity of each battery. Jan's [13, 14] structures had the ability to reconfigure structures with variant batteries in series to reach the voltage requirements during electric vehicle charging, which constantly change. The structure proposed by Visairo et al.[11], as shown in Figure 1a, can change the system's output voltage based on load conditions, thereby reducing the power loss of the voltage regulator during the power supply process and improving energy utilization efficiency. For the same purpose to enhance the energy efficiency of the system, Lawson et al. [15] and He et al. [16] also proposed simplified structures which has less switches than Visairo's design. Kim et al. [17] improved the system's ability to recover from battery failures by introducing multiple ports to the structure. The complex structure between batteries and switches enables the flexibility of RBS, but also brings the challenges in design and control of system. Thus, several approaches to analyze the RBS structure and performance have been proposed in the literature to tackle these challenges. For instance, Han et al.[18] derived an analytical expression for the maximum switch current during battery system reconfiguration for a specific RBS structure. This helps guide the selection of switches and provide support for the hardware design of RBS. Chen et al.[19] proposed a systematic approach based on the sneak circuit theory to fundamentally avoid the short-circuit problem of reconfigurable battery systems. They thoroughly analyzes all paths between the cathode and anode of each battery in the RBS and identifies paths that only contain switches as short-circuit paths for pre-checking before system reconfiguration.

In spite of maximum switch current mentioned above, the maximum allowable current (MAC), defined as the maximum current allowed by system under the constraints of the battery cell, is another critical indictor of RBS that need to be evaluated during the design or control process of system. It helps the designers to assess whether the RBS meets the output current requirements, and contribute to the formulation of appropriate and safe management strategies for the battery management system (BMS). Unfortunately, few studies on the RBS structure analysis have been conducted to determine the MAC of RBSs. A intuitive and straightforward method is to enumerate all possible switch states and calculate the output current of the system under each reconfigurated structure. But this method is inefficient and time-consuming, especially for RBSs with a large number of switches.

To solve this issue, a new method to effectively evaluate the MAC of RBS is proposed in this paper. First, a greedy algorithm is designed to search the possible circuit topology of RBS with MAC effciently. Meanwhile, an improved direct graph model, considering the voltage, internal resistance, and maximum allowable current of the battery, and the external load, is porposed to obtain the accurate current value of RBS under specific circuit topology. To the best of our knowledge, the present work is the first to develop an efficient calculation method of RBS MAC. The main contributions of the paper can be summarized as follows:

- Proposing a effective method to determine the MAC of RBSs with arbitrary structures, including scenarios with isolated batteries.

- Application of the greedy algorithm to solve the MAC problem, whose computational complexity is greatly reduced compared with the brute force algorithm.

- introducing an improved directed graph model, considering the voltage, internal resistance, and maximum allowable current of the battery, and the external load, to achieve the current analysis of the RBS.

The remainder of this paper is organized as follows: Section II presents the framework and details of the proposed directed graph model and the greedy algorithm. Section III demonstrated a case study of using the proposed method to determine the MAC of a novel and complex structure. The calculation results, the algorithm's computational complexity and scenarios such as batteries isolation also are discussed. Finally, the concluding remarks are drawn in Section IV.

2 Methodology

The central principle of this method is to make the batteries in RBS connected in parallel as much as possible, thereby maximizing the output current of the RBS. To universally and automatically achieve this, the overall process is divided into four steps, as shown in Figure 2. Firstly, a directed graph model is established for subsequent computations. The model not only contains the connected relationships between batteries and switches, but also retains the performance parameters of the batteries. Subsequently, based on the equivalent circuit, the MAC problem is transformed into specific objective functions and constraints. Then, the shortest paths (SPs, where additional batteries and switches on the path are penalized as distance) for the batteries are obtained using the Dijkstra algorithm to guide the batteries in the RBS connect in parallel. Finally, a greedy algorithm is employed to organize the switches, allowing the batteries to connect via their SPs while satisfying the constraints, resulting in the MAC of the RBS.

Step 1: build directed graph model

- Connected relationships
- Batteries performance parameters

Step 3: search shortest path

$$\omega(p) = N_s \cdot n_b(p) + n_s(p)$$

- Dijkstra algorithm

Step 2: obtain constraints and objective function

$$\max \quad \eta(\boldsymbol{X}_s)$$
$$\text{s.t.} \max(\boldsymbol{I}_b) \leq I_m,$$

Step 4: solve MAC greedily

- Switches state $\boldsymbol{X}_s$
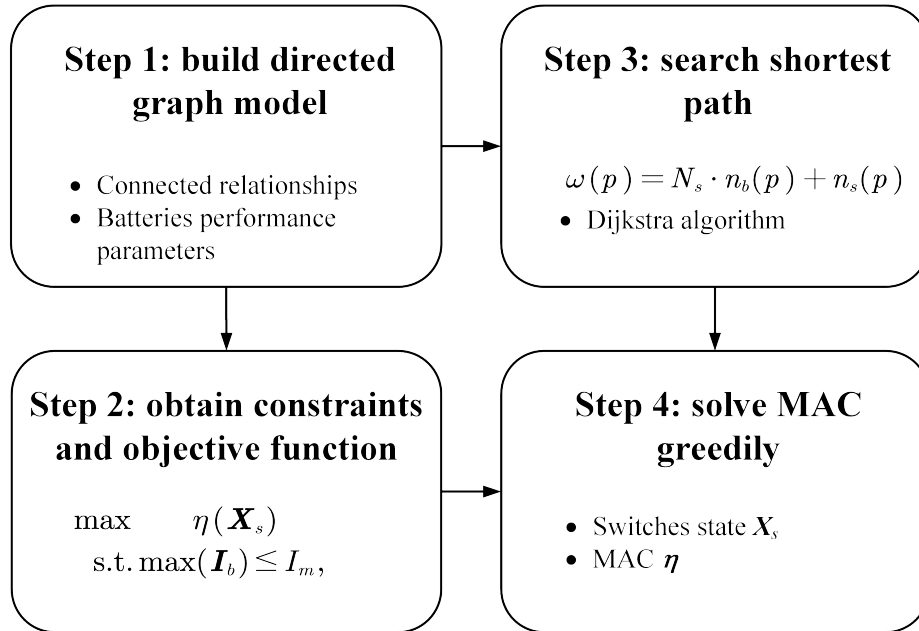- MAC $\boldsymbol{\eta}$

Figure 2: Diagram of this method, which contains four main steps.
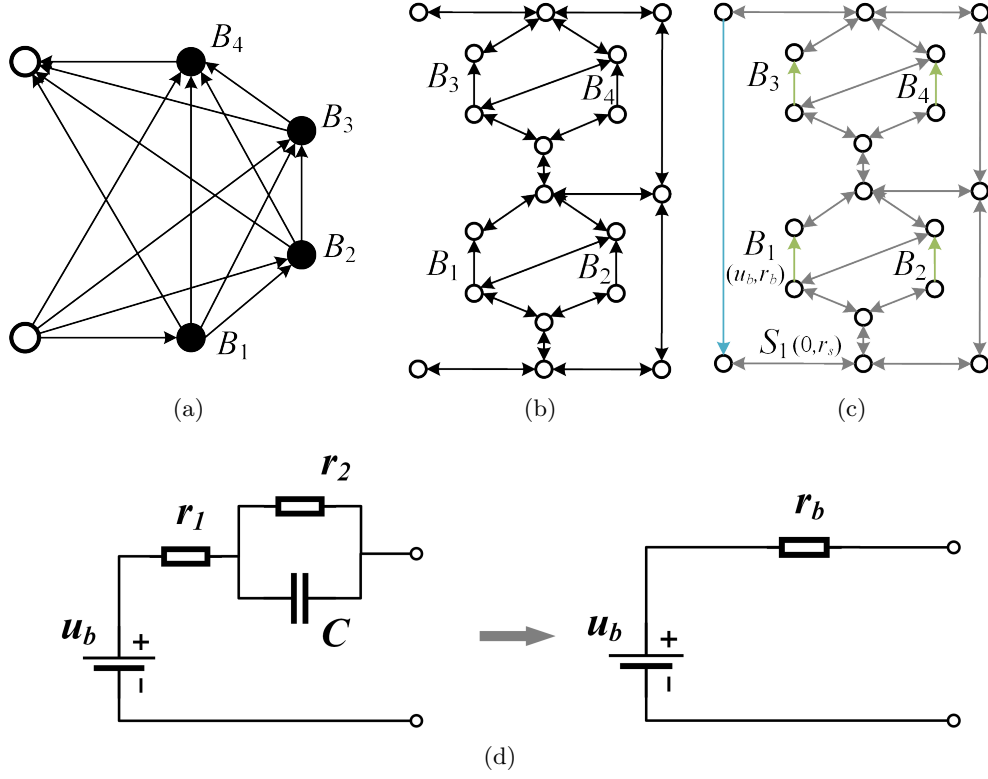
2.1 Directed graph Model

Figure 3: Directed graph models used in (a) He's work [20], (b) our previous work , and (c) the improved model in this paper. (d) The equivalent circuit of a battery in this method.

He et al. [20] once proposed an abstracted directed graph model for RBS, where the nodes represented the batteries, the edges represented the configuration flexibility, and the weight of each vertex corresponded to the battery voltage (Figure 3a). The model effectively captured all potential system configurations and offered a direct metric for configuration flexibility, but it did not specify the physical implementation of the connectivity between batteries, meaning one graph might correspond to multiple RBS structures. We previously proposed a novel directed graph model that, completely different from He's model, used nodes to represent the connections between batteries and switches, and directed edges to represent batteries and switches (Figure 3b), allowing for a one-to-one correspondence between the RBS structure and the directed graph model. This model was able to accurately and comprehensively represent the RBS topological structure but could not be used for quantitative MAC calculations due to the lack of consideration on the voltage, internal resistance and maximum allowable current of the battery. To address this, an improvement on our previous model is conducted by adding electromotive force and resistance attributes on the edges based on its equivalent circuits . The model also considers the external load as an equivalent resistance and integrate it into the analysis, making it a complete circuit model for later circuit analysis. Figure ?? The following will provide a detailed explanation of the method for equating the components in

RBS and constructing the directed graph model.

In order to use circuit analysis methods to solve the MAC of the RBS, the components in the RBS are equated to ideal circuit elements. For instance, as shown in Figure 3d, the battery in the RBS can be represented as a black-box circuit consisting of two resistors (i.e., r_1 and r_2) and a capacitor (i.e., C), known as the Thevenin model[21, 22]. With an emphasis on the stable output of the RBS, the capacitor in the Thevenin model can be considered as an open circuit without affecting the steady-state current. Therefore, the battery i in the RBS can be simplified as the series connection between a constant voltage source u_i and a resistor r_i. Furthermore, the state of switch j in the RBS is represented by a binary variable x_j, where 0 is for ON and 1 is for OFF, respectively. When the switch is closed, it can be regarded as a resistor with a very small resistance value r_j. Lastly, the external load is considered as a resistor with a value of R_o.

For a given RBS structure, its directed graph model $G(V, E)$ is constructed as follows:

1. Nodes: The nodes in the directed graph correspond to the connection points of components in the actual RBS. Assuming there are a total of N nodes in the RBS, for the sake of convenience, the anode of the RBS is denoted as v_1 and the cathode as v_N.

2. Edges: The edges in the directed graph correspond to the batteries, switches, and external electrical loads in the actual RBS. Therefore, there are three types of directed edges. For a battery B_i, its directed edge e_i is drawn from the cathode to the anode, as the battery only allows current to flow in one direction when in operation. For a switch S_j, since it is allowed to work under bi-directional currents, it is represented by a pair of directed edges with two-way directions. Regarding the external electronic load, as it is connected to the anode and cathode of the RBS, a directed edge from v_N to v_1 is used to represent it. In conclusion, for a given RBS structure with N_b batteries and N_s switches, the total number of directed edges is $N_b + 2N_s + 1$, where 1 refers to the external electrical load.

3. Edges' attributes: Each edge is assigned two attributes, voltage difference and resistance, based on the equivalent method mentioned above. The values for the battery B_i, switch S_j, and external loads correspond to (u_i, r_i), $(0, r_j)$, and $(0, R_o)$, respectively.

2.2 Constraints and Objective Function

For a given RBS, determination of its MAC involves maximizing the RBS output current while ensuring that the currents of all batteries do not exceed the batteries' maximum allowable current. In this subsection, the constraints and objective function to solve the RBS's MAC will be established through circuit analysis, based on its directed graph model provided in the previous subsection.

First, the topology in the directed graph model is represented in matrix form $\boldsymbol{A}$, known as the incidence matrix , defined in Equation 1.

$$a_{kl} = \begin{cases} 1, & \text{edge } l \text{ leaves node } k, \\ -1, & \text{edge } l \text{ enters node } k, \\ 0, & \text{otherwise.} \end{cases} \tag{1}$$

6

For a directed graph consisting of N nodes and $N_b + 2N_s + 1$ directed edges, its incidence matrix $\boldsymbol{A}$ is an $N \times (N_b + 2N_s + 1)$ matrix. In this matrix, the rows and columns represent the nodes and edges of the directed graph, respectively. By distinguishing the components in the RBS corresponding to each column , $\boldsymbol{A}$ can be rewritten as:

$$\boldsymbol{A} = \begin{bmatrix} \boldsymbol{A}_b & \boldsymbol{A}_s & \boldsymbol{A}_o \end{bmatrix}, \tag{2}$$

where $\boldsymbol{A}_b$, $\boldsymbol{A}_s$ and $\boldsymbol{A}_o$ are the sub-matrices corresponding to the batteries, switches and external electrical load, respectively. To alleviate computational complexity, matrix $\boldsymbol{A}$ undergoes dimensionality reduction. Since each directed edge has one node to leave and one to enter, the sum of the values in every column of $\boldsymbol{A}$ is zero. Therefore removing the last row will not result in a loss of information. On the other hand, since each switch in the RBS is represented by a pair of directed edges with two-way directions, the two columns corresponding to the switch are mutually opposite. Thus, for the sub-matrix $\boldsymbol{A}_s$, only one column is retained for each pair of columns representing the same switch. As a result, $\boldsymbol{A}$ can be reduced to a $(N-1) \times (N_b + N_s + 1)$ matrix, denoted as $\tilde{\boldsymbol{A}}$, for further calculation of current and voltage. Similar to Equation 2, $\tilde{\boldsymbol{A}}$ can be rewritten as:

$$\tilde{\boldsymbol{A}} = \begin{bmatrix} \tilde{\boldsymbol{A}}_b & \tilde{\boldsymbol{A}}_s & \tilde{\boldsymbol{A}}_o \end{bmatrix}. \tag{3}$$

After obtaining the incidence matrix, the currents of all batteries and output in RBS are determined by solving the circuit equations. According to Kirchhoffs law, we have

$$\begin{cases} \tilde{\boldsymbol{A}}\boldsymbol{I} = \boldsymbol{0}, \\ \boldsymbol{U} = \tilde{\boldsymbol{A}}^{\mathrm{T}}\boldsymbol{U}_n, \end{cases} \tag{4}$$

where $\boldsymbol{I}$ and $\boldsymbol{U}$ indicate the current and voltage difference arrays of the $N_b + N_s + 1$ edges, respectively; $\boldsymbol{U}_n$ is the voltage array of the $N-1$ nodes. These directed edges are treated as generalized branches and expressed in matrix form as follows

$$\boldsymbol{I} = \boldsymbol{Y}\boldsymbol{X}\boldsymbol{U} - \boldsymbol{Y}\boldsymbol{X}\boldsymbol{U}_s + \boldsymbol{I}_s, \tag{5}$$

where $\boldsymbol{U}_s$ and $\boldsymbol{I}_s$ denote the source voltage and source current of the generalized branches, respectively. Because all batteries have been equivalent to voltage sources rather than current sources in the previous subsection, all elements of the array $\boldsymbol{I}_s$ are 0, while the elements of the array $\boldsymbol{U}_s$ are equal to the first attribute of the corresponding edges in the directed graph. The $\boldsymbol{Y}$ in Equation 5 is the admittance matrix of the circuit, defined as the inverse of the impedance matrix. The elements on the diagonal of matrix $\boldsymbol{Y}$ are equal to the reciprocal of the resistance, which is the second attribute of the corresponding edges in the directed graph, and the off-diagonal elements $\boldsymbol{Y}$ are 0. The $\boldsymbol{X}$ is the state matrix, which describes whether the RBS batteries and switches are allowed to

pass current. It is defined as

$$\boldsymbol{X} = \text{diag}(\underbrace{1, 0 \cdots, 1}_{N_b \text{ of } 0/1}, \underbrace{1, 0 \cdots, 1}_{N_s \text{ of } 0/1}, 1) = \begin{bmatrix} \boldsymbol{X}_b & & \\ & \boldsymbol{X}_s & \\ & & 1 \end{bmatrix}. \tag{6}$$

Where the elements x_i of the matrix $\boldsymbol{X}_b$ represent whether the battery i has been removed from the circuit, with $x_i = 1$ indicating removal and $x_i = 0$ indicating that it is still available to supply power. When all batteries are health and capable of providing current to the external load, $\boldsymbol{X}_b$ is an identity matrix. The elements x_j of the matrix $\boldsymbol{X}_s$ represent whether the switch j is closed, with $x_j = 1$ indicating closure and $x_j = 0$ indicating disconnection, which is consistent with the previous subsection.

Theoretically, the output current I_o and the currents of each battery $\boldsymbol{I}_b$ in the RBS can be determined by solving Equations 4, 5, and 6 under any given state $\boldsymbol{X}$. In order to obtain specific constraint conditions and objective functions, it is further assumed that all batteries have the same electromotive force and internal resistance, denoted as u_b and r_b, respectively. This allows for the derivation of explicit expressions for I_o and $\boldsymbol{I}_b$. After derivation and simplification, the output current I_o and the currents of each battery $\boldsymbol{I}_b$ are ultimately represented as Equations 7 and 8, respectively.

$$I_o = \frac{1}{R_o r_b} \tilde{\boldsymbol{A}}_o^{\mathrm{T}} \boldsymbol{Y}_n^{-1}(\boldsymbol{X}) \tilde{\boldsymbol{A}}_b \boldsymbol{U}_b, \tag{7}$$

$$\boldsymbol{I}_b = \frac{1}{r_b^2} [\tilde{\boldsymbol{A}}_b^{\mathrm{T}} \boldsymbol{Y}_n^{-1}(\boldsymbol{X}) \tilde{\boldsymbol{A}}_b \boldsymbol{U}_b - r_b \boldsymbol{U}_b], \tag{8}$$

where $\boldsymbol{U}_b$ is a $N_b \times 1$ array with all elements equaling to u_b; $\boldsymbol{Y}_n$ is the equivalent admittance matrix of the circuit, defined as

$$\boldsymbol{Y}_n(\boldsymbol{X}) = \frac{1}{R_o} \tilde{\boldsymbol{A}}_o \tilde{\boldsymbol{A}}_o^{\mathrm{T}} + \frac{1}{r_b} \tilde{\boldsymbol{A}}_b \boldsymbol{X}_b \tilde{\boldsymbol{A}}_b^{\mathrm{T}} + \frac{1}{r_s} \tilde{\boldsymbol{A}}_s \boldsymbol{X}_s \tilde{\boldsymbol{A}}_s^{\mathrm{T}}. \tag{9}$$

To characterize the current output capacity of the RBS structure under different switching states, an indicator η is defined by the ratio of I_o and $\max(\boldsymbol{I}_b)$ shown in Equation 10:

$$\eta = \frac{I_o}{\max(\boldsymbol{I}_b)}. \tag{10}$$

Finally the problem of solving MAC can be formulated as

$$\max \eta(\boldsymbol{X}_s) \tag{11}$$

$$\text{s.t.} \max(\boldsymbol{I}_b) \leq I_m, \tag{12}$$

where I_m is the maximum allowable current of the battery.

However, it is still computationally difficult to solve 11 because of the $\boldsymbol{Y}_n^{-1}$. On one hand, due to the introduction of nonlinear terms by $\boldsymbol{Y}_n^{-1}$, many effective methods in linear optimization are not suitable for this scenario. On the other hand, the rank of Y_n is proportional to the number

of batteries and switches, which can be very large for a large RBS system, leading to significant computational burden. Therefore, intelligent algorithms that rely on evolving by iteration may face efficiency problem when dealing with large RBS system. In order to address this issue, the problem should be considered from the perspective of guiding the RBS to reconstruct as many parallel structures as possible. Consequently, a greedy algorithm based on the shortest path is proposed. The detailed implementation process is presented in the following two subsections.

2.3 Shortest Path

The path p used in this method is defined as the complete route that passes through one battery (or a consecutive series of batteries) and closed switches, connecting the anode v_1 to the cathode v_N of the RBS. By applying a penalty to the series-connected batteries on the path, where additional batteries imply a longer distance, the algorithm encourages the RBS to form parallel structures as much as possible. Meanwhile, to reduce the number of switches controlled during the reconstruction process, a penalty is also applied to the total number of switches on the path, while ensuring the minimum number of batteries. Therefore, the distance ω of the path p is defined by the following equation:

$$\omega(p) = N_s \cdot n_b(p) + n_s(p), \tag{13}$$

where N_s is the total number of switches in the system; $n_b(p)$ and $n_s(p)$ are number of batteries and switches in the path p respectively. Moreover, the shortest path SP_i is defined as the path with the minimum ω for battery i, as shown in the following equation:

$$SP_i = \underset{p \in P_i}{\arg\min}\, \omega(p), \tag{14}$$

where P_i is the set of all paths from v_1 to v_N which pass through the directed edge i.

The SP_i can be solved by the Dijkstra algorithm. The Dijkstra algorithm is a graph search method that finds the shortest path between two given nodes in a weighted graph, efficiently solving the single-source shortest path problem. Assuming that the cathode and anode of battery i are denoted as v_i^- and v_i^+ respectively, the path p of battery i can be divided into three segments : $v_1 \to v_i^-$, $v_i^+ \to v_N$, and $v_i^- \to v_i^+$. The $v_i^- \to v_i^+$ is the directed edge corresponding to battery i. With the Dijkstra algorithm, shortest paths for the $v_1 \to v_i^-$ and $v_i^+ \to v_N$ can be calculated under the weights given in Equation 13, denoted as $SP(v_i^- \to v_i^+)$ and $SP(v_i^+ \to v_N)$, respectively. Finally, the SP_i for battery i is formed by the complete path with $SP(v_1 \to v_i^-)$, $v_i^- \to v_i^+$, and $SP(v_i^+ \to v_N)$.

2.4 Greedy Algorithm

From the perspective of series/parallel connections, integrating more batteries into the circuit through their shortest paths (SPs) results in a larger number of batteries connected in parallel, thereby increasing the total output current of the RBS. However, conflicts may arise between the SPs of different batteries. For instance, the SPs of two batteries might form a short-circuited RBS

structure, which is not allowed. To address this issue, a greedy algorithm is employed to incorporate as many SPs as possible while satisfying the reconstruction requirements.

The algorithm, as illustrated in Figure 4, can be summarized as follows, with the corresponding pseudo-code presented in Algorithm 1. First, the shortest paths (SPs) are obtained using Equations 13 and 14 in conjunction with Dijkstra Search. Next, the matrix $\boldsymbol{A}$ is calculated using Equation 1, and the initial N_{set} is set to N_b. The algorithm iteratively checks different combinations of c_b batteries from N_b and updates N_{set} using a dichotomy method until convergence is reached. For each combination, the algorithm constructs an effective solution if possible, and calculates the currents I_o and $\boldsymbol{I}_b$ using Equations 7 and 8. If the maximum current $\boldsymbol{I}_b$ is less than or equal to I_m, the η is calculated using Equation 10, and the maximum η is updated accordingly. Finally, the algorithm outputs the maximum η once N_{set} converges.

3 Case Study

3.1 Structures

Currently, two types of RBS structures have been proposed by Visairo et al. [11] and Lawson et al. [15], both of which have been practically used. The primary goal of Visairo's structure (Figure 5b) was to achieve dynamic adjustment of RBS output power; however, the isolation of unhealthy batteries was not sufficiently addressed in their work. Lawson et al. designed the RBS structure shown in Figure 5a for the purpose of battery isolation. This structure has the advantage of easily isolating batteries, but it cannot dynamically adjust the output current of RBS. Based on the structures of Visairo and Lawson, this paper presents a new structure, as shown in Figure 5c. By integrating the Visairo RBS structure into the Lawson RBS structure, the new structure not only allows the flexibility to switch the batteries between series, parallel, and mixed series-parallel modes, but also easily enables the isolation of highly degraded batteries from the RBS. And their variations in output current under battery isolation conditions will be studied. This RBS structure will be used to validate the effectiveness of the proposed method for calculating the MAC, and be compared with the Lawson's and Visairo's structure to illustrate its advantage on battery isolation.

3.2 Result

As shown in Figure 5c, the new RBS structure consists of 4 batteries and 19 switches. The corresponding directed graph is depicted in Figure 6a, which is composed of a total of 18 nodes and 43 edges. Batteries B_1, B_2, B_3, and B_4 are denoted by green directed edges in the graph, while the 19 switches are represented by gray directed edges with bi-directional arrows. The external electrical load is treated as a directed edge from the cathode of the RBS (i.e., node 18) to the anode (i.e., node 1), as indicated by the blue directed edge in the graph. Utilizing Equation 13 and the Dijkstra algorithm, the SPs of the four batteries in the RBS structure of Figure 5c are highlighted by red in Figures 6b-6e. Finally, the MAC calculation results of the structure in Figure 5c are shown as Table 1 and Figure 6f, obtained by the greedy algorithm 1. Table 1 contains the switches states, the output current I_o, battery current $\boldsymbol{I}_b$ and ratio η of the RBS structure with all batteries in good

```
                    ┌─────────────────────────┐
                    │  Input: RBS structure   │
                    └────────────┬────────────┘
                                 ↓
                    ┌─────────────────────────┐
                    │ get SPs by Equations    │
                    │    13 and 14 and        │
                    │    Dijkstra Search      │
                    └────────────┬────────────┘
                                 ↓
                    ┌─────────────────────────┐
                    │    get A from           │
                    │    Equation 1           │
                    └────────────┬────────────┘
                                 ↓
                    ┌─────────────────────────┐
                    │  init N_set = N_b       │
                    └────────────┬────────────┘
                                 ↓
    ┌─────────────────────────┐      ┌──────────────────┐
    │  get c_b s by com-      │◄─────│  reset N_set by  │
    │   binating N_set        │      │    dichotomy     │
    │  batteries from N_b     │      └──────────────────┘
    └────────────┬────────────┘              ↑ No
                 ↓
        ◇ are all c_b s checked? ◇──Yes──► ◇ is N_set converged? ◇──Yes──►┌──────────────┐
                 │                                                         │ Output: max η│
                 │ No                                                      └──────────────┘
                 ↓
    ┌─────────────────────────┐
    │   select an unchecked   │
    │   c_b, and get its X_m  │
    │  by if switch j ∈ ∪...  │
    │  X[j] = 1 else 0        │
    └────────────┬────────────┘
                 ↓
    ┌─────────────────────────┐
    │ get Y_n by Equation 9   │
    └────────────┬────────────┘
                 ↓
        ◇ is Y_n invertible? ◇──No──►┌──────────────────┐
                 │                    │  construct an ef-│
                 │ Yes                │  fective solution│
                 ↓                    └──────────────────┘
    ┌─────────────────────────┐
    │  get I_o and I_b by     │◄──────────────┘
    │   Equations 7 and 8     │
    └────────────┬────────────┘
                 ↓
        ◇ is max I_b ≤ I_m? ◇──No──►┌──────────────┐
                 │                   │  drop this η │
                 │ Yes               └──────────────┘
                 ↓
    ┌─────────────────────────┐
    │ get η by Equation 10    │
    └────────────┬────────────┘
                 ↓
    ┌─────────────────────────┐
    │    update max η         │◄──────────────┘
    └─────────────────────────┘
```
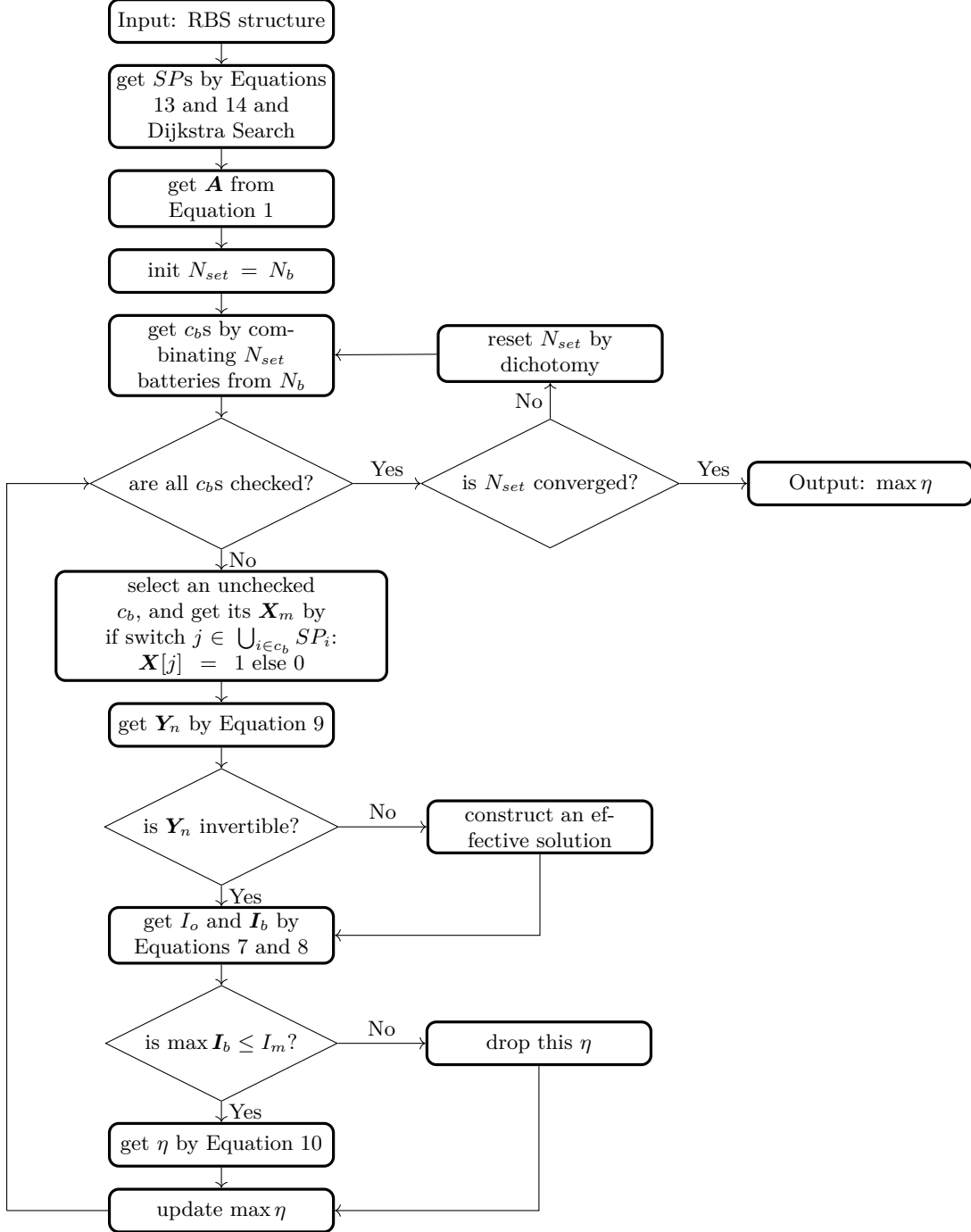
Figure 4: The computational flowchart of the MAC for a given RBS.
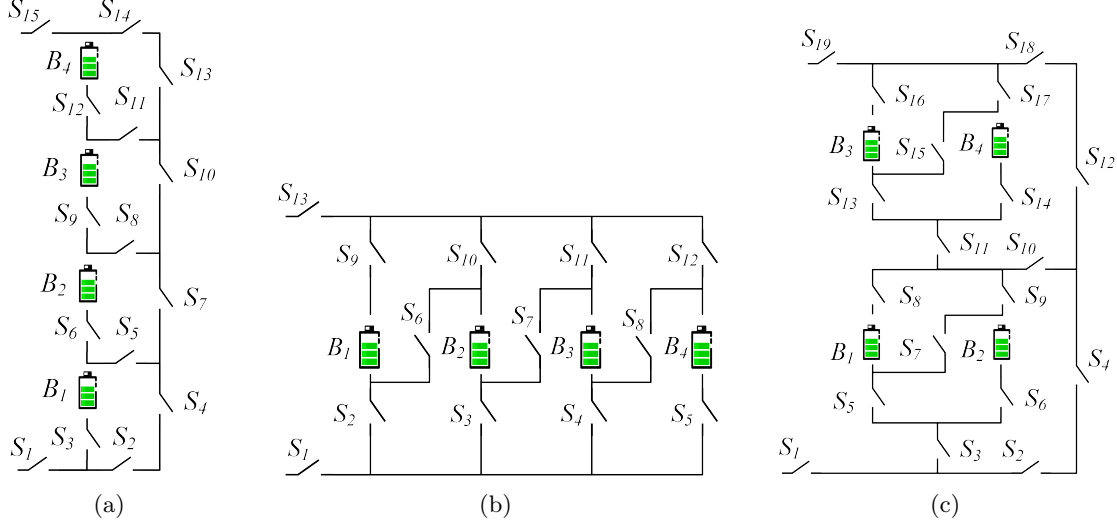
Figure 5: The 4-battery RBS structures proposed by (a)Lawson[15], (b)Visairo[11] and (c)this paper.

health when the RBS output reaches the MAC. Figure 6f presents the corresponding circuit, with the red highlight indicating that current is flowing through the respective branches.

Table 1: MAC Calculating result of the 4-battery RBS structure in Figure 5c.

Structure	Figure 5c with 4 batteries and 19 switches
Switch ON	$S_1,S_3,S_5,S_6,S_8,S_9,S_{10},S_{12},S_{18},S_{19}$
I_o	$2u_b/(2R_o+r_b)$
$\boldsymbol{I}_b$	$[u_b/(2R_o+r_b),u_b/(2R_o+r_b),0,0]$
$\max\eta$	2

Similarly, the MAC calculation results of the structures in Figures 5a and 5b are shown as Table 2 and Table 3, respectively. In order to verify and compare the results from the greedy algorithm, we also utilized a brute force algorithm that go through all possible switch states to calculate the MAC of the same three RBS. For a given RBS structure with N_s switches, the final max η is the maximum of ηs from all 2^{N_s} reconfigured structures. The final results are the same as the results shown in Tables 1-3. It is worth noting that the method used the greedy algorithm only calculated 11, 11, and 1 reconfigured structures for the RBS structure in Figures 5c, 5a, 5b, respectively. While for the same RBS, the method counted all possible switch states computed 2^{19}, 2^{15}, and 2^{13} structures, respectively.

Furthermore, the RBS with isolated batteries is taken into consideration and calculated. The MAC calculation results for the three structures under study, with varying numbers of isolated batteries, are presented in Table 4. Figures 7a-7d illustrate the corresponding switch control schemes for the new structure proposed in this paper under different isolated battery conditions.
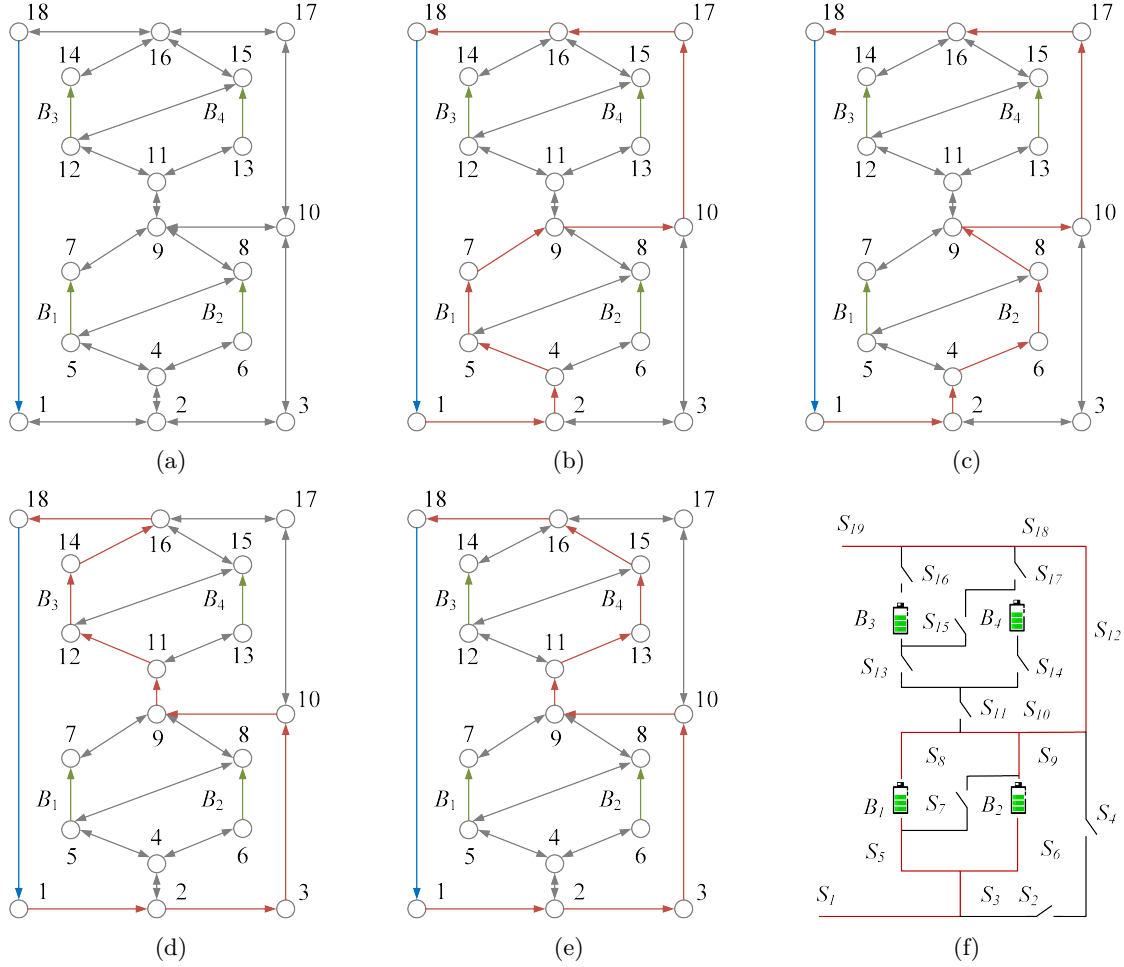
12

Figure 6: For the RBS structure in Figure 5c, (a)its directed graph and the SPs (highlighted in red) of battery (b)B_1, (c)B_2, (d)B_3, (e)B_4. (f)The circuit of the RBS with its output reaching the MAC.

Table 2: MAC Calculating result of the 4-battery RBS structure in Figure 5a.

Structure	Figure 5a with 4 batteries and 15 switches
Switch ON	$S_1,S_3,S_5,S_7,S_{10},S_{13},S_{14},S_{15}$
I_o	$u_b/(R_o + r_b)$
$\boldsymbol{I}_b$	$[u_b/(R_o + r_b), 0, 0, 0]$
$\max\eta$	1

Table 3: MAC Calculating result of the 4-battery RBS structure in Figure 5b.

Structure	Figure 5b with 4 batteries and 13 switches
Switch ON	$S_1,S_2,S_3,S_4,S_5,S_9,S_{10},S_{11},S_{12},S_{13}$
I_o	$4u_b/(4R_o + r_b)$
$\boldsymbol{I}_b$	$[u_b/(4R_o + r_b), u_b/(4R_o + r_b), u_b/(4R_o + r_b), u_b/(4R_o + r_b)]$
$\max\eta$	4

13

Table 4: The variation of MAC with the number of isolated batteries for different RBS structures, including the structure proposed by Lawson et al., Visairo et al. , and the structure proposed in this paper.

number of isolated batteries	η of RBS structure		
	our	Visairo's	Lawson's
0	2	4	1
1	2	3	1
2	2^{a} or 1^{b}	2	1
3	1	1	1

[a] isolate two batteries within the same substructure, as shown in Figure 7b
[b] isolate one battery in each of the two substructures, as shown in Figure 7c
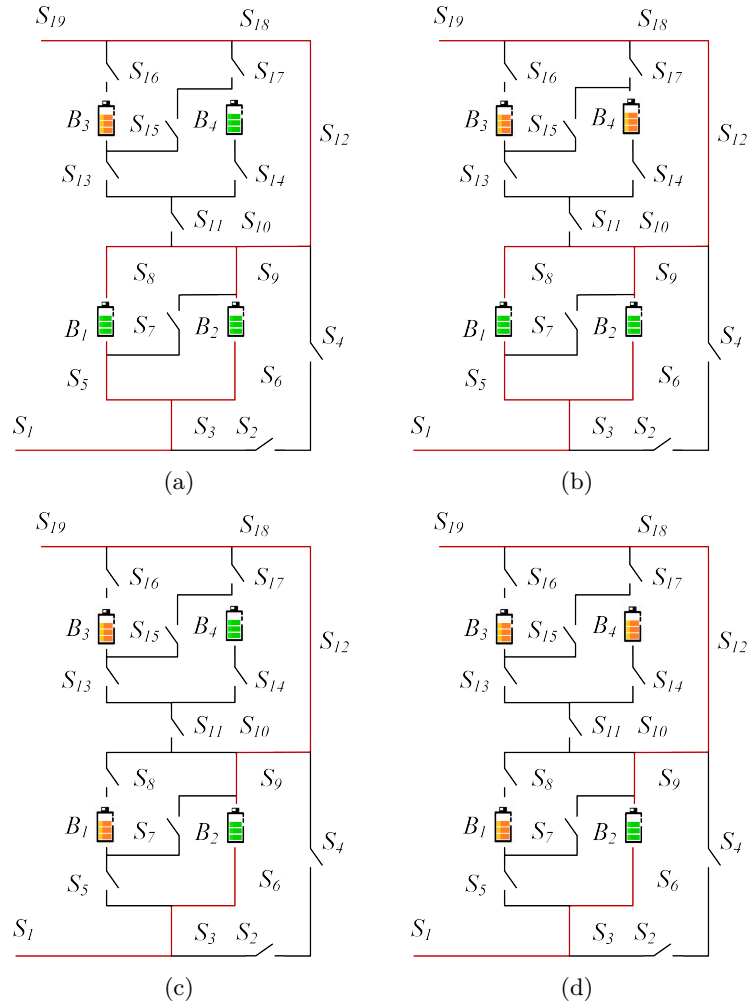
Figure 7: The circuit states of MACs when isolating (a)one, (b)two(best case), (c)two(worst case) and (d)three batteries for the structure in Figure 5c.

3.3 Discussion

As shown in Figure 6 and Table 1. When B_1 and B_2 or B_3 and B_4 are connected in parallel, the RBS can output the maximum current, which is $\eta = 2$, i.e., twice the current output of a single battery in RBS. Adding more batteries to the main circuit can only form a series structure and will not improve the MAC. Therefore, the switches state given in Table 1 can make the RBS output current reach the maximum. The results of MAC obtained by brute force algorithm method is identical to the one by the greedy algorithm.

From the literature research we have conducted, no formal report on the algorithm for MAC in RBS has been found yet. The brute force algorithm, which goes through all possible switch states, is the most straightforward way to solve the MAC problem and is used as a benchmark for the proposed greedy algorithm. Assuming that a RBS has N_b batteries and N_s switches, and the corresponding directed graph has N nodes, it requires 2^{N_s} iterations to traverse all reconfigured structures. The calculation for each reconfigured structure by Equations 7-10 requires matrix inversion and matrix multiplication, with a time complexity of $O(N^3 + 2N^2 N_b + N^2 N_s + N N_b^2)$. Therefore, the time complexity of the brute force algorithm is $O(2^{N_s}(N^3 + 2N^2 N_b + N^2 N_s + N N_b^2))$. The greedy algorithm proposed in this paper requires find the SP for each battery, which requires N_b iterations. Each SP can be obtained by couple Dijkstra algorithms. Therefore, the total time complexity of calculating all SPs is $O(2N_b(N_b + 2N_s) \log N)$. According to the Appendix 1, the RBS can reconfigure $C_{N_b}^{N_{set}}$ structures by selecting N_{set} batteries from N_b batteries, which is $\sum_{N_{set}=1}^{N_b} C_{N_b}^{N_{set}}/N_b \approx 2^{N_b}/N_b$ on average. Hence, with bisection method, the time complexity of the greedy algorithm is $O(2^{N_b}/N_b(N^3 + 2N^2 N_b + N^2 N_s + N N_b^2) \log N_b + 2N_b(N_b + 2N_s) \log N)$, i.e., $O(2^{N_b}/N_b(N^3 + 2N^2 N_b + N^2 N_s + N N_b^2) \log N_b)$. Based on currently proposed RBS structures[23–28], the number of batteries N_b, switches N_s, and nodes N have the following quantitative relationships: $N_s \approx (3 \sim 5)N_b$, $N \approx N_s$. After simplifying, the time complexity of the greedy algorithm is $O(2^{N_b} N_s^2 \log N_b)$, while it is $O(2^{N_s} N_s^3)$ for brute force algorithm. Therefore, it is reasonable to believe that as the size of the RBS increases, especially the number of the switches, the greedy algorithm will have an advantage over the algorithm that goes through all reconfigured structures. This can be confirmed from the number of structures required for MAC determination in the previous subsection. Compared to the brute force algorithm, the efficiency of the method based on the greedy algorithm has been improved by 3000 to 48000 times, which is theoretically $N_s 2^{N_s - N_b} \log N_b$ times according to the above time complexity analysis. Among the three RBS structures, the highest is the RBS structure with 19 switches (Figure 5c). This benefit from two key points: (1) The SPs guide the RBS to reconfigure reasonable structures, rather than blindly going through all possible structures. This reduces the factor in complexity from 2^{N_s} to 2^{N_b}, which is the main reason for the improvement in efficiency; (2) The bisection method further accelerates this process. However, the greedy algorithm proposed in this paper still contains exponential terms in the time complexity, which means it may not be able to handle extremely large-scale RBS structures.

It is important to note that η is used as the objective function instead of I_o in solving MAC. This choice makes the result of MAC more reasonable. As shown in Table 1, I_o and $\boldsymbol{I}_b$ are functions of R_o, u_b, and r_b. However, when I_o was used as the objective function, even for the same RBS

structure, the MAC solution and corresponding switches state could change due to different external electrical appliances. It would increase the difficulty and uncertainty in RBS structure design. In order to eliminate the influences of such a problem, η, which is the ratio of I_o and max $\boldsymbol{I}_b$, is adopted as the objective function in our research. η solely reflects the maximum output current capability of the RBS structure. Assuming that the maximum allowed current of batteries in the RBS is I_m, the maximum output current of the RBS structure can be calculated as ηI_m by determining the η of the structure.

The method proposed in this paper is significant for the design of RBSs in the following aspects. Most of the currently proposed RBS structures[23–28] exhibit simple topological characteristics, and the calculation of MACs is relatively straightforward, even intuitive. However, these simple structures do not always fully satisfy the requirements of complex applications, such as dynamically adapting the circuit to variable and random operating conditions, and actively equalizing differences among the batteries in the RBS. Moreover, isolation of the batteries disrupts the original regularity and symmetry of the topology, which complicates the otherwise simple structure, and the maximum output current of the system becomes more challenging to obtain. On the contrary, the proposed method can be employed to calculate the MAC of arbitrary RBS structures, especially for these above complex and flexible RBS structures.

To illustrate this point, the MACs of three RBS structures mentioned above are calculated after one and more batteries are isolated, as shown in Table 4. Specifically, for the structure presented in Figure 5c, the corresponding circuit states of MACs of isolating one to three batteries are depicted in Figures 7a-7d. This structure has two cases of isolating two batteries: one is to isolate two batteries within the same substructure (Figure 7b), in which case $\eta = 2$; the other is to isolate one battery in each of the two substructures (Figure 7c), in which case $\eta = 1$. From the results shown in Figure 7a-7d, it can be observed that the proposed method provides reasonable outcomes for isolating batteries with any number and position.

Furthermore, the output current for the three RBS with isolated batteries is also shown in Table 4. For the structure proposed by Lawson et al., the MAC is independent on the number of isolated batteries. However, for Visairo's structure, the MAC decreases with the increasing number of isolated batteries. Nevertherless, the MAC of the structure proposed in this work is positioned between these above two structures. This indicates that the structure proposed in this paper, compared to Lawson's structure, has a larger MAC under the same number of batteries, and exhibits a wider output current regulation range.

4 Conclusion

This paper proposes a pervasive and automatic method for computing the MAC of a given RBS efficiently. The method is implemented by a greedy algorithm combined with a directed graph model which considers the voltage, internal resistance, and maximum allowable current of the batteries, as well as the external load. The main advantage of this method is its ability to calculate the MAC of RBSs with arbitrary structures. Even in the scenarios with random isolated batteries, the method remains effective. Compared with the brute force algorithm, the proposed method has

16

higher computational efficiency under the same calculation results. This is achieved by two key points when constructing the greedy algorithm: (1) Calculate the shortest path of each battery by Dijkstra algorithm to obtain the SP of each battery; (2) determine the maximum number of available batteries by bisection method to reduce the computational complexity. This method helps to fully tap the current output potential of the RBS, guide the RBS structure design and optimization in the design stage, and assist in evaluating the current overload risk of the system in practical applications.

5 Appendix

Algorithm 1: Get the max available currents of a certain RBS

Data: Directed graph model $G(V, E)$ of the RBS

Result: $\max \eta$

1 for $i \in E_b$ **do**

2 $P_i \leftarrow \{path|$starts at v_1 and ends at $v_n\}$;

3 $SP_i \leftarrow p_i$ which has the minimum $\omega(p_i)$ among all $p_i \in P_i$.

4 end

5 get $\boldsymbol{A}$ by Equation 1;

6 while *not yet determine* $\max \eta$ **do**

7 $N_{set} \leftarrow$ number of setected SPs calculated by dichotomy;

8 $C_b \leftarrow$ set of all combinations of N_{set} batteries from N_b;

9   **for** $c_b \in C_b$ **do**

10 $\boldsymbol{x}_s \leftarrow$ list of all switches' state: $x_s[j] = 1$ if $j \in \bigcup_{i \in c_b} SP_i$ else 0;

11 $\boldsymbol{X} \leftarrow diag[1, 1, \cdots, 1, \boldsymbol{x}_s]$;

12   get $\boldsymbol{Y}_n$ by Equation 9;

13   **if** $\boldsymbol{Y}_n$ *is invertible* **then**

14   pass

15   **else**

16   construct an effective solution

17   **end**

18   get I_o by Equation 7;

19   get $\boldsymbol{I}_b$ by Equation 8;

20   **if** $\max(\boldsymbol{I}_b) \leq I_m$ **then**

21 $\eta \leftarrow I_o / \max(\boldsymbol{I}_b)$;

22   **else**

23   break

24   **end**

25   **end**

26 end

Acknowledgments

Author Contributions

B. Xu conceived the main idea, formulated the overarching research goals and aims, designed the algorithm, and reviewed and revised the manuscript. G. Hua developed and analyzed the model, implemented the code and supporting algorithms, and wrote the initial draft. C. Qian provided critical review, commentary, and revisions. Q. Xia contributed to shaping the research, analysis, and manuscript. B. Sun conducted the research and investigation process. Y. Ren secured the funding and supervised the project. Z. Wang verified the results and provided necessary resources.

Funding

Conflicts of Interest

The authors declare that there is no conflict of interest regarding the publication of this article.

Data Availability

This work does not require any data to be declared or publicly disclosed.

References

1. de Siqueira LMS and Peng W. Control Strategy to Smooth Wind Power Output Using Battery Energy Storage System: A Review. Journal of Energy Storage 2021;35:102252.

2. Yang Y, Bremner S, Menictas C, and Kay M. Battery Energy Storage System Size Determination in Renewable Energy Systems: A Review. Renewable and Sustainable Energy Reviews 2018;91:109–25.

3. Cho J, Jeong S, and Kim Y. Commercial and Research Battery Technologies for Electrical Energy Storage Applications. Progress in Energy and Combustion Science 2015;48:84–101.

4. Zhang L. Development and Prospect of Chinese Lunar Relay Communication Satellite. Space: Science & Technology 2021;2021.

5. Schwanbeck E and Dalton P. International Space Station Lithium-ion Batteries for Primary Electric Power System. In: *2019 European Space Power Conference (ESPC)*. IEEE, 2019:1–1. DOI: 10.1109/ESPC.2019.8932009.

6. Yang N, Zhang X, Shang B, and Li G. Unbalanced Discharging and Aging Due to Temperature Differences among the Cells in a Lithium-Ion Battery Pack with Parallel Combination. Journal of Power Sources 2016;306:733–41.

7. Feng F, Hu X, Hu L, Hu F, Li Y, and Zhang L. Propagation Mechanisms and Diagnosis of Parameter Inconsistency within Li-Ion Battery Packs. Renewable and Sustainable Energy Reviews 2019;112:102–13.

8. Jeevarajan JA and Winchester C. Battery Safety Qualifications for Human Ratings. Interface magazine 2012;21:51–5.

9. Pombo DV. A Hybrid Power System for a Permanent Colony on Mars. Space: Science & Technology 2021;2021.

10. Han W, Wik T, Kersten A, Dong G, and Zou C. Next-Generation Battery Management Systems: Dynamic Reconfiguration. IEEE Industrial Electronics Magazine 2020;14:20–31.

11. Visairo H and Kumar P. A Reconfigurable Battery Pack for Improving Power Conversion Efficiency in Portable Devices. In: *2008 7th International Caribbean Conference on Devices, Circuits and Systems*. IEEE, 2008:1–6. DOI: `10.1109/ICCDCS.2008.4542628`.

12. Ci S, Zhang J, Sharif H, and Alahmad M. A novel design of adaptive reconfigurable multicell battery for power-aware embedded networked sensing systems. In: *IEEE GLOBECOM 2007-IEEE Global Telecommunications Conference*. IEEE. 2007:1043–7.

13. Engelhardt J, Gabderakhmanova T, Rohde G, and Marinelli M. Reconfigurable Stationary Battery with Adaptive Cell Switching for Electric Vehicle Fast-Charging. In: *2020 55th International Universities Power Engineering Conference (UPEC)*. 2020:1–6. DOI: `10.1109/UPEC49904.2020.9209774`.

14. Engelhardt J, Zepter JM, Gabderakhmanova T, Rohde G, and Marinelli M. Double-string battery system with reconfigurable cell topology operated as a fast charging station for electric vehicles. Energies 2021;14:2414.

15. Lawson B. A Software Configurable Battery. EVS26 International Battery, Hybrid and Fuel Cell Electric Vehicle Symposium 2012.

16. He L, Kong L, Lin S, et al. Reconfiguration-assisted charging in large-scale lithium-ion battery systems. In: *2014 ACM/IEEE International Conference on Cyber-Physical Systems (ICCPS)*. IEEE. 2014:60–71.

17. Kim H and Shin KG. On dynamic reconfiguration of a large-scale battery system. In: *2009 15th IEEE Real-Time and Embedded Technology and Applications Symposium*. IEEE. 2009:87–96.

18. Han W, Kersten A, Zou C, Wik T, Huang X, and Dong G. Analysis and estimation of the maximum switch current during battery system reconfiguration. IEEE Transactions on Industrial Electronics 2021;69:5931–41.

19. Chen SZ, Wang Y, Zhang G, Chang L, and Zhang Y. Sneak Circuit Theory Based Approach to Avoiding Short-Circuit Paths in Reconfigurable Battery Systems. IEEE Transactions on Industrial Electronics 2021;68:12353–63.

20. He L, Gu L, Kong L, Gu Y, Liu C, and He T. Exploring Adaptive Reconfiguration to Optimize Energy Efficiency in Large-Scale Battery Systems. In: *2013 IEEE 34th Real-Time Systems Symposium*. 2013:118–27. DOI: `10.1109/RTSS.2013.20`.

21. He H, Xiong R, Zhang X, Sun F, and Fan J. State-of-Charge Estimation of the Lithium-Ion Battery Using an Adaptive Extended Kalman Filter Based on an Improved Thevenin Model. IEEE Transactions on Vehicular Technology 2011;60:1461–9.

22. Mousavi G. S and Nikdel M. Various Battery Models for Various Simulation Studies and Applications. Renewable and Sustainable Energy Reviews 2014;32:477–85.

23. Ci S, Zhang J, Sharif H, and Alahmad M. A Novel Design of Adaptive Reconfigurable Multicell Battery for Power-Aware Embedded Networked Sensing Systems. In: *IEEE GLOBECOM 2007-2007 IEEE Global Telecommunications Conference*. 2007:1043–7. DOI: 10.1109/GLOCOM.2007.201.

24. Alahmad M, Hess H, Mojarradi M, West W, and Whitacre J. Battery Switch Array System with Application for JPL's Rechargeable Micro-Scale Batteries. Journal of Power Sources 2008;177:566–78.

25. Kim H and Shin KG. Dependable, Efficient, Scalable Architecture for Management of Large-Scale Batteries. In: *Proceedings of the 1st ACM/IEEE International Conference on Cyber-Physical Systems*. ICCPS '10. New York, NY, USA: Association for Computing Machinery, 2010:178–87. DOI: 10.1145/1795194.1795219.

26. Kim Y, Park S, Wang Y, et al. Balanced Reconfiguration of Storage Banks in a Hybrid Electrical Energy Storage System. In: *2011 IEEE/ACM International Conference on Computer-Aided Design (ICCAD)*. 2011:624–31. DOI: 10.1109/ICCAD.2011.6105395.

27. Kim T, Qiao W, and Qu L. A Series-Connected Self-Reconfigurable Multicell Battery Capable of Safe and Effective Charging/Discharging and Balancing Operations. In: *2012 Twenty-Seventh Annual IEEE Applied Power Electronics Conference and Exposition (APEC)*. 2012:2259–64. DOI: 10.1109/APEC.2012.6166137.

28. He L, Kong L, Lin S, et al. Reconfiguration-Assisted Charging in Large-Scale Lithium-ion Battery Systems. In: *2014 ACM/IEEE International Conference on Cyber-Physical Systems (ICCPS)*. 2014:60–71. DOI: 10.1109/ICCPS.2014.6843711.